Case Studies in Construction Materials 20 (2024) e03088

Contents lists available at ScienceDirect

Case Studies in Construction Materials

journal homepage: www.elsevier.com/locate/cscm

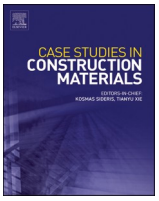

Mobilizing railway track stability with nonionic cement asphalt mortar for floating sleeper mitigation – 2D/3D numerical investigation and full-scale testing verification

Dae-Wook Park [a], Chanyong Choi [b], Tam Minh Phan [a], Tri Ho Minh Le [c,*]

[a] Dept. of Civil Engineering, Kunsan National University, 558 Daehak Ro, Kunsan, Jeonbuk, South Korea
[b] Korea Railway Research Institute, 176 Cheldo bangmulgwan-ro, Uiwang, Gyeonggi-do, South Korea
[c] Faculty of Civil Engineering, Nguyen Tat Thanh University, 300A Nguyen Tat Thanh Street, District 4, Ho Chi Minh City 70000, Viet Nam

ARTICLE INFO

Keywords:
Railway track stabilization
CAM reinforcement
Floating sleeper mitigation
2D/3D simulation insights
Full-scale testbed

ABSTRACT

This study addresses the mitigation of the floating sleeper phenomenon in ballasted railway tracks through the implementation of Nonionic Cement Asphalt Mortar (CAM). Full-scale testing experiments evaluate track performance with and without CAM stabilization, revealing its efficacy in forming a robust membrane between ballast particles to reinforce the track-bed structure. Wheel load modeling, including static and dynamic, train movement modeling, roadbed pressure analysis, distribution of load, and track rigidity analysis. Life Cycle Cost Analysis (LCCA) establishes CAM's cost-effectiveness by significantly reducing settlement and ensuring long-term durability. Numerical simulations using ABAQUS demonstrate CAM's effectiveness in stabilizing deteriorated ballast. Furthermore, the simulations prove capable of detecting the floating sleeper phenomenon in the full-scale test bed, offering valuable insights into real-world applications. Both 2D and 3D modeling consistently show a more than 30% reduction in initial settlement and a 0.5 mm displacement in CAM-reinforced ballast compared to controls. Plastic displacement in new ballast is consistently 50% less in the initial 50,000 cycles, with ultimate plastic settlement reduced by 40%, indicating the robustness of CAM across different modeling dimensions. The dataset analysis identifies a floating sleeper issue, evidenced by pressure variations in deteriorated ballast. In the control and simulation sections, there is a pressure drop from 65 kPa to 28 kPa, while the reinforced section maintains stable pressures (50 kPa, 36.5 kPa, 10 kPa) with closely aligned predicted values. Despite pressure reduction in simulated zones, the dataset strongly supports concerns about the substantial pressure decrease due to the floating sleeper phenomenon. LCCA substantiates CAM's economic advantage, showcasing a 79.7% cost reduction over 60 years, endorsing CAM as a sustainable maintenance strategy. In conclusion, CAM stabilization effectively mitigates the floating sleeper effect, ensuring long-term track durability, and providing valuable contributions to sustainable railway infrastructure design and maintenance practices.

* Corresponding author.
E-mail address: lhmtri@ntt.edu.vn (T.H. Minh Le).

https://doi.org/10.1016/j.cscm.2024.e03088
Received 8 January 2024; Received in revised form 21 February 2024; Accepted 24 March 2024
Available online 27 March 2024

1. Introduction

Railway tracks, serving as the lifeline of efficient transportation systems, underpin numerous industries and are indispensable for global goods and passenger movement [1]. Ensuring the continued integrity and functionality of these tracks presents a crucial challenge for railway engineers. The ballast, composed of crushed stone or gravel, is pivotal in distributing train loads and upholding track stability [2]. It absorbs dynamic forces, prevents track subsidence, and preserves proper alignment. A particularly challenging area is the track transition zone, where different track structures converge, adding complexity to railway engineering. Hölscher and Meijers [3] highlight the imperative of understanding track and soil behavior in these zones. Studies by Berggren [2] and Gallage et al. [4] emphasize the pivotal role of track stiffness in the long-term degradation of track quality. Research by Lee et al. [4], Le et al. [5], and Wang et al. [6] addresses dynamic behavior, material suitability, and the influence of moisture conditions in transition zones, underlining the necessity to consider environmental factors. Costa D'Aguiar et al. [7] and Paixão et al. [7] unravel the complexities of transition zones, emphasizing the impact of backfill settlements on train/track interaction. These findings underscore the urgency for robust ballast stabilization and reinforcement strategies to ensure the resilience and durability of railway infrastructure at transition zones. The challenges associated with railway track stabilization have been the subject of considerable investigation in the literature. In the realm of railway track stabilization, recent techniques often grapple with prolonged curing periods, posing a challenge to efficient and timely stabilization processes [8]. Notably, there is a growing concern regarding the applicability of these methods primarily at the initial construction stage rather than during routine maintenance, limiting their adaptability and overall efficacy [9]. Additionally, the inherent stiffness of certain materials intended for stabilization can become a double-edged sword. Some materials exhibit excessive rigidity, compromising the desired flexibility and elasticity required for optimal track performance, while others, although designed to be stiff, may become prone to cracks and structural vulnerabilities [10]. Addressing these contemporary challenges is crucial for advancing the field and propelling the development of effective, adaptable, and durable railway track stabilization techniques.

However, despite its significance, ballast is susceptible to a phenomenon known as the "floating sleeper [11,12]." The "floating sleeper" issue occurs when the ballast particles under the sleeper become loose and displaced (as shown in Fig. 1), leading to a non-uniform distribution of load. This phenomenon compromises the integrity of the track structure, resulting in reduced stability, increased maintenance needs, and potential safety hazards [2]. As a result, railway operators are compelled to invest considerable resources in regular maintenance and tamping processes to restore the desired track condition. Traditionally, track stabilization methods have relied on tamping—lifting the track, inserting fresh ballast, and compacting it to achieve the required stability. While tamping is effective in the short term, it is a labor-intensive and costly process. Furthermore, its effects are often short-lived, as the "floating sleeper" issue tends to resurface over time.

The pursuit of robust and sustainable railway track stabilization has prompted diverse explorations in research and engineering. Recent advances encompass geosynthetic materials, synthetic fibers, polymers, and additives like cement and asphalt emulsions, each designed to address specific challenges in ballast stabilization [13,14]. Mechanized systems, including continuous track monitoring and automated tamping machines, further contribute to this multi-dimensional field's evolution. This overview sets the stage for the novel approach introduced in this study, emphasizing the growing significance of varied methods to stabilize ballast. Concurrently, Cement Asphalt Mortar (CAM) has gained prominence as a versatile solution in engineering applications [8,10]. Recent research efforts have enhanced CAM properties and extended their utility, especially in road construction, pavement rehabilitation, and railway track stabilization [8,15]. This section provides insights into the evolving landscape of CAM research, highlighting its versatility and potential contributions to sustainable infrastructure solutions, and emphasizing its use in railway track stabilization [15,16].

The utilization of CAM or Cement Emulsified Asphalt Mortar (CEA) presents innovative solutions for track stabilization. Researchers like Ma et al. [13] and Li et al. [17,18] explored the preparation and characterization of CAM and its effectiveness in reducing settlement and enhancing durability. Saesaei et al. [14] extended the focus to eco-friendly CEA mortar, evaluating its fracture toughness and durability properties. Numerical studies by Jiang et al. [9] and Yuan et al. [9] reviewed the factors influencing the performance of CAM, while Najjar et al. [14,19] investigated the mixed mode-I/II fatigue performance of CAM, providing valuable insights into its durability. The application of CAM in real-world scenarios is validated by Le et al. [20], who conducted a full-scale testing performance evaluation, emphasizing CAM's effectiveness in ballasted track stabilization. These studies collectively

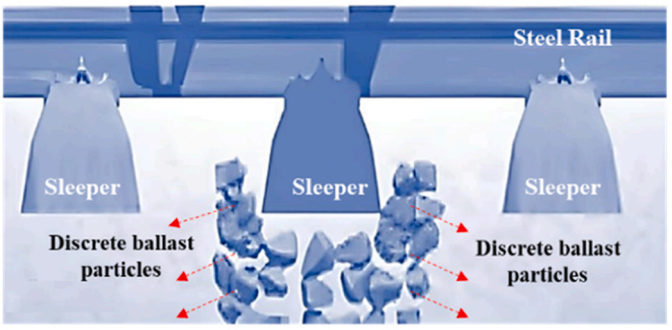

Fig. 1. Illustration of the floating sleeper/discrete ballast after dynamic load.

contribute to advancing the understanding and practical implementation of innovative materials like CAM and CEA for sustainable railway infrastructure [21–23].

In the realm of railway track stabilization, persistent challenges remain despite advancements and the adoption of CAM. Existing techniques like tamping and mechanical compacting face limitations in long-term performance, load distribution, and maintenance. To address these issues, our research introduces a novel approach leveraging CAM's unique properties. Our focus centers on mitigating the critical concern of floating sleepers, aiming to improve load distribution, enhance track stability, and reduce maintenance demands. The study includes a comparative assessment of CAM stabilization in two ballast types: original clean and dusted. By examining CAM's effectiveness in these scenarios, we contribute valuable insights to optimize track performance and durability. This research pioneers innovative methods to address gaps in railway track stabilization techniques and offers solutions to tackle the floating sleeper phenomenon.

The manuscript presents a comprehensive exploration of novel techniques to address the challenges inherent in railway track stabilization. With a focus on enhancing track stability and longevity, this research investigates the application of CAM as a stabilizing agent. The manuscript is structured to provide an in-depth analysis of the findings through a multi-faceted approach. The subsequent sections provide detailed insights into the materials and methods used in the study, including components of the numerical simulations and full-scale test bed verifications. The core of the manuscript centers on the results and discussions section, which presents and analyzes the research outcomes. Special attention is given to the impact of floating sleepers and the comparison between clean ballast and dusted ballast when using CAM. The manuscript concludes with a synthesis of the findings and their implications for the field, highlighting contributions to addressing the critical challenge of railway track stabilization.

2. Materials and methods

2.1. Materials

2.1.1. Cement asphalt mortar (CAM

CAM serves as a pivotal component in the stabilization of ballasted railway tracks. This unique material is formulated by blending asphalt emulsion and cement, offering distinct properties that are instrumental in enhancing track performance. The tested properties of the material met the specified requirements as follows [5,20]: Viscosity at 25℃ was 5.5, within the range of 2–30. Sieve residue (1.18 mm) was 0.2%, well below the maximum limit of 0.3%. Storage stability after 24 hours was 0.05%, below the allowed threshold of 1%. Evaporation residue, presented as a percentage by mass, exceeded the required 57%, measuring at 60.2%. Penetration at 25℃ was 75, falling within the range of 60–300. Ductility at 15℃ surpassed the minimum requirement of 40, achieving a value higher than 120. The toluene-soluble fraction was 98.5%, surpassing the specified threshold of 97%.

This study outlines the composition of Cement Asphalt Mortar (CAM) in terms of the percentage by cement mass. The formulation consists of 30% cement (C), 7.6% quick-hardening additive (QA), 30% asphalt emulsifier (AE) (*), 20% sand (S), 10% water (W), 2% superplasticizer (SP), and 0.1% defoaming agent (D). The general characteristics of the CAM mixture, as detailed in Table 1, are further presented for reference [5,20]. [5,20].

The composition of CAM involves the precise blending of asphalt emulsion and cement in specified ratios, resulting in a durable and robust mixture. The density, curing time, durability, adhesive properties, and rheological behavior of CAM play a critical role in its performance as a stabilizing agent for railway tracks.

2.1.2. Nonionic, Cationic, and Anionic CAM

In Section 2.1.1, the focus is on CAM, a versatile material renowned for its efficacy in stabilizing ballasted railway tracks. The CAM mixture in this research is evaluated by ASTM D244 [24], ASTM C191 [25], ASTM C1097 [26], and Korea standard in asphalt mixture (KSF 2374[27]). CAM is further differentiated based on the type of asphalt emulsion incorporated, categorizing it into Nonionic, Cationic, and Anionic CAM [24]. Nonionic CAM, using neutral asphalt emulsions, is compatible with diverse aggregates, forming strong bonds for enhanced track stability. Cationic CAM, with positively charged emulsions, suits scenarios requiring compatibility with negatively charged aggregates, ensuring a durable track structure. Anionic CAM, utilizing negatively charged emulsions, addresses positively charged aggregates for robust track stabilization. This system underscores CAM's crucial role in maintaining stable and durable railway tracks with effective, tailored solutions.

Table 1
General properties of CAM mixture.

Properties	Mixing Stability (Residue Content)	Flowability (Flow Cone Test)	2-Hour Compressive Strength	28-Day Compressive Strength
Residue Content	Lower than 1%	-	-	-
Flow Cone Test	-	17–19 sec (s)	-	-
2-Hour Compressive Strength	-	-	~3.2 MPa	-
28-Day Compressive Strength	-	-	-	~6.5–7.5 MPa

Table 2
Properties of Additives Used in Cement Asphalt Mortar.

Additive	Chemical Composition	Appearance	Color	Particle Size	Melting Point (°C)	Boiling Point (°C)	Density (g/cm^3)	Solubility	Compatibility	Dosage
Quick Hardening Powder (White Cement)	Varies based on white cement	Fine powder	Varies depending on the type	Varies depending on the type	Varies	Varies	Varies	Insoluble in water	Generally compatible with mortar materials	As per project needs
Silica Fume Powder	Silica (SiO_2)	Fine powder	Gray	1–100 nanometers	Approx. 1713	Approx. 2230	2.2–2.4	Insoluble in water	Generally compatible with cementitious materials	As per project needs
Sand	Silica-based minerals	Granular, fine particles	Varies depending on the type	0.0625–2 millimeters (mm)	Approx. 1700	Varies	Varies	Insoluble in water	Generally compatible with mortar materials	As per project needs
Superplasticizer	Polycarboxylate compounds	Liquid or powder	Varies depending on the type	Varies depending on the type	N/A	N/A	Varies	Soluble in water	Generally compatible with mortar materials	As per project needs
Anti-Foaming Powder (Aluminum)	Aluminum powder or particles	Fine powder or particles	Silver-gray to white	Varies depending on the product	Approx. 660	Approx. 2519	Approx. 2.7	Insoluble in water	Generally compatible with various materials	As per project needs

2.1.3. Additives

In the domain of CAM, the incorporation of specific additives is instrumental in shaping its performance. Notably, the quick hardening admixture, white cement, is a vital component with distinctive properties, including a rapid setting time and strengthening capabilities [28]. Commonly used in CAM, white cement accelerates the stabilization of railway tracks, particularly in scenarios requiring prompt attention. Silica Fume Powder, characterized by a high specific gravity and fine particle size, is a crucial additive in CAM known for enhancing material strength, and durability, and reducing permeability [15]. Adding 8% of Silica Fume Powder by weight has been observed to optimize these properties effectively. Sand, a fundamental ingredient, contributes to CAM's workability and stability. Incorporating fine-grained sand in the range of 30–35% by weight establishes a robust matrix within CAM, thereby enhancing its mechanical properties. The addition of Superplasticizer, an essential CAM component, significantly improves flowability and workability [29]. Optimal results have been achieved with a dosage of 1.5% Superplasticizer by weight of cement. Moreover, Anti-Foaming Powder (Aluminum) is employed to reduce foam and bubbles in the CAM mixture. A recommended dosage of 0.2% Anti-Foaming Powder by weight ensures consistent mortar quality during mixing and application [23]. These specific values underscore the critical role of each additive in CAM, providing a nuanced understanding of their contributions to the material's properties. Table 2 presents the overview of the materials used to develop the final CAM mixture used in this study.

2.1.4. Instrumentation setup

The instrumentation configuration was designed to accommodate high-frequency data acquisition, reaching up to 500 Hz, utilizing a data logger with a socket compatible with both earth pressure gauges and vertical displacement gauges. For static tests, the measurement data storage interval was set to 1 Hz, while dynamic tests required a higher frequency, ranging from 500 to 1000 Hz.

The data logger, interfaced with a PC and controlled by a dedicated program, was equipped with ample storage capacity to ensure seamless data acquisition and storage. The sensor array was strategically positioned to capture and analyze sleeper and rail conditions in response to variations in roadbed pressures. Elastic and plastic displacements of the track system were quantified for comprehensive analysis.

Roadbed pressure was measured using pressure sensors, commonly referred to as tonometers, as Fig. 2 illustrates. These sensors were carefully set up below sleepers and rails on the roadbed level underneath the loading bed. More precisely, the center of the sleeper or loading point at position 1 was 65 cm away from the pressure sensors at position 2. In the same manner, the distance between those at position 3 and the middle sleeper was 130 cm. This purposeful configuration was created to elucidate the properties of load distribution through the observation of changes in roadbed pressure.

2.1.4.1. Data logger. A sophisticated data logger system was deployed for precise data acquisition, supporting a sampling frequency exceeding 500 Hz. For static tests, the storage interval for measurement data was configured at 1 Hz, ensuring accurate capture of static conditions. In dynamic testing scenarios, the data logger operated at an increased frequency of 500 Hz, facilitating the meticulous recording of dynamic responses within the system.

2.1.5. Mixing, application, and casting of CAM

Drawing upon the collective expertise of the author team and insights gleaned from previous works [5,20], the wet-mixing method was selected for its proven efficacy. In this meticulous process, dry components, including cement, quick-hardening admixture, and silica fume, are initially combined with water and superplasticizer (W + SP) at a shearing rate of 120 rpm for approximately 2 minutes. This initial stage results in the formation of a stable cement paste.

Next, asphalt emulsion is added to the pre-mixed cement paste along with a specified additive. For an extra minute, the amalgamation proceeds at the same shearing rate. The purposeful use of the wet-mixing technique is to guarantee the stability of asphalt droplets inside the emulsion and inhibit the development of CAM particles that are too large.

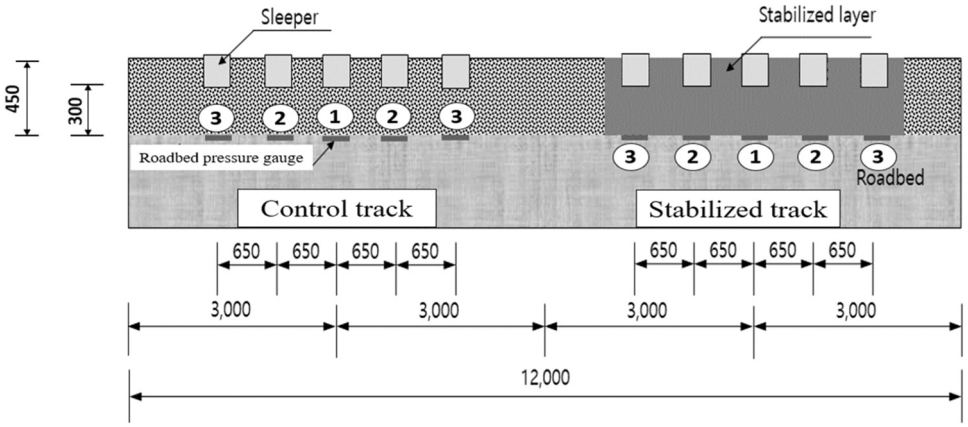

Fig. 2. Location for installing earth pressure gauges.

The newly made CAM mixture is then directly poured onto the surface of the ballast layer, resulting in a smooth transition to the ballast-stabilizing phase. This method makes use of the increased flowability that CAM mixes naturally possess. Pouring is precisely timed to coincide with the subterranean locations of pressure sensors, making comparisons easier later on.

The necessary CAM volume is 7.5% of the ballast content to provide the best uniformity and efficient interaction among the ballast granules, based on preliminary experiences and mock-up tests [21,22]. The remaining CAM mixture after stabilization is set aside for rheology testing and poured into 50 ×100 mm Unconfined Compression Strength (UCS) molds for further testing in the lab. Fig. 3 presents an overview of the final test setup.

2.1.6. Dynamic load test assessment approach

2.1.6.1. Dynamic wheel load computation. The static and dynamic loads utilized in evaluating the "control" track and the "CAM-reinforced" track conform to the prescribed standards of the KRL-2012 for train loads [30], as detailed in the Korean standard (KR C-14030) [31–33]. Within the context of this comprehensive testbed, designed for assessing the real-world performance of the railway infrastructure, a mixed-use scenario involving both passenger and cargo transport is simulated. The dynamic wheel loads are presented in Fig. 4, ensuring a representative and reliable estimation of the loads acting on the tracks.

The evaluation of static and dynamic loads for both the "control" track and the CAM-reinforced track adheres to the guidelines outlined in KRL-2012 [30]. The standard train load equations, as stipulated in the Korean standard [31], are employed for load application. The testing is conducted on a full-scale testing utilizing the general railroad, accommodating both passengers and cargo. The main railroad is used as full-scale testing for the evaluation, which can accommodate passengers as well as freight. The conventional train load chart, shown in Fig. 4, is used to determine the dynamic load on the wheels for this condition.

In order to accurately replicate the actions of a moving train, the dynamic wheel load (P_{dyn}) is calculated using an extensive formula that also takes into account the effective wheel load (P_{eff}) while the dynamic amplitude factor is named DAF. For roadbed fundamental computations, the typical variation weight is always set to 1, and the coefficient depends on the track condition that is being considered.

Designing velocities that are considered include those that apply to passenger-cargo trains (at 100, 120, 140, and 160 km/h) as well as commuter trains (at 250, 300, and 350 km/h). The DAF multiplied by the P_{eff}, as shown in Eq. (1), yields the highest P_{dyn} that is supposed to be used throughout the loading test.

The equation for P_{dyn} is expressed as $P_{eff} \times DAF$, as presented in Eq. (1). Here, P_{eff} signifies the effective wheel load and is calculated by multiplying the static wheel load (P_{st}) by a factor of 1.2. The DAF is determined based on the train speed (V) and is subject to different formulas for various speed ranges. For speeds up to 60 km/h, DAF is defined as 1 plus the product of t (weight of standard deviation) and ∅ (coefficient dependent on track quality). In the case of passenger trains traveling at speeds between 60 and 350 km/h, the DAF incorporates additional adjustments to account for speed variations. Similarly, for passenger combined cargo trains in the speed range of 60–160 km/h, the DAF formula involves modifications based on speed parameters. The coefficients t and ∅ are associated with the weight of standard deviation and track quality, respectively, with a confidence interval probability of 1 ($t = 1$)

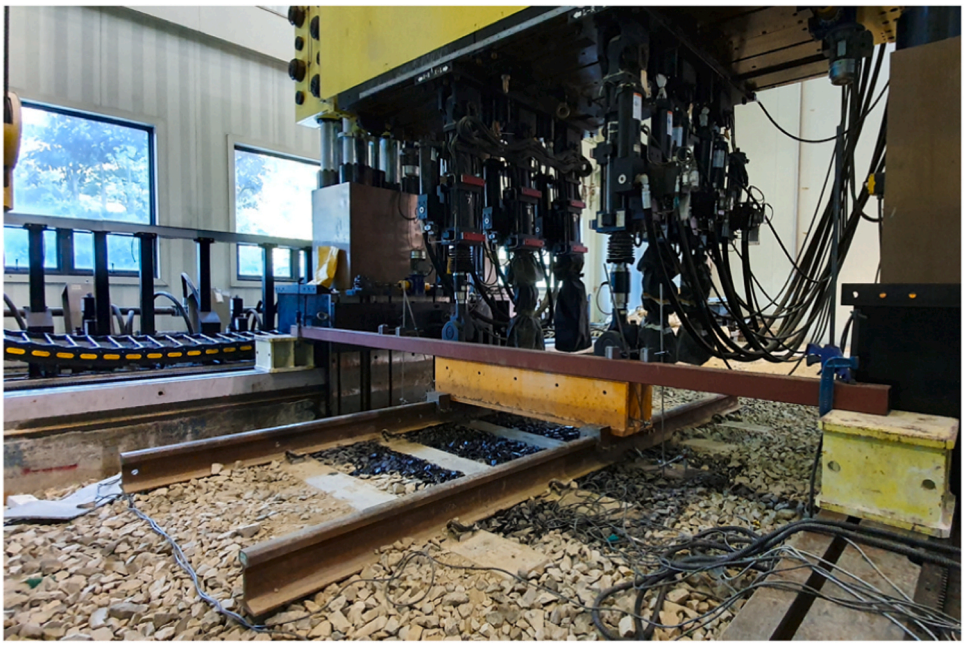

Fig. 3. Construction of Testbed and Measurement Instruments setup.

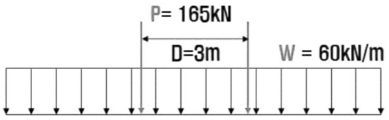

Fig. 4. Loading condition showing KRL-2012 Standard Train Load Diagram (Passenger Line).

applied to roadbed calculations.

$$P_{dyn} = P_{eff} \times DAF \quad (1)$$

The design specifications for KRL-2012 in the category of mixed passenger and cargo lines with a V of 100 km/h are outlined based on the suggestion from the KRL standard [30]. The static wheel load (P_{st}) is set at 110 kN, and the associated DAF is determined to be 1.250. The effective wheel load (P_{eff}) is calculated by multiplying the static wheel load by a factor of 1.2, resulting in 132 kN. The dynamic wheel load (P_{dyn}) is subsequently determined as 165 kN. These parameters collectively establish the design criteria for the KRL-2012 category, ensuring the stability and functionality of the railway system for mixed passenger and cargo lines at a speed of 100 km/h.

The probability assignments for different applications and track conditions are detailed in the following content. At a probability level of 68.3%, application 1 focuses on contact stress and subgrade performance, particularly in track conditions classified as "Very good," with a corresponding coefficient of 0.1. For a higher probability of 95.4%, application 2 addresses lateral load and ballast bed considerations in tracks categorized as "Good," utilizing a coefficient of 0.2. The most critical scenarios, with a probability of 99.7%, involve application 3, which examines rail stresses, fastenings, and supports in track conditions labeled as "Bad," with an associated coefficient of 0.3. These probability assignments serve as a guide for prioritizing and addressing specific aspects of railway track maintenance and performance based on varying degrees of track quality.

For the calculation of the maximum design dynamic wheel load, parameters such as a train speed of 140 km/h, a standard deviation weight (t) of 1, and a track quality coefficient (∅) of 0.2 were employed in this study. In order to guarantee a balanced implementation and comply with pragmatic concerns, the ultimate dynamic wheel load utilized in the static load test was modified to 165 kN. In order to accommodate for the estimated highest dynamic wheel load of 165 kN while sustaining a regulated load increase/decrease intensity of roughly 20 kN, the static load test was carried out with a load set at 200 kN. Furthermore, the loading frequency was determined to be 8 Hz, taking into account the train speed and the spacing of the Boogie. This meticulous approach to load specification guarantees a comprehensive evaluation of the track's response to dynamic loading conditions.

2.1.6.2. Dynamic load test method. With an intended stress of 95 kN ± 70 kN, the dynamic load assessments, as shown in Fig. 5, were carefully designed for sine wave loads that range from 25 kN to 165 kN. Remarkably, the dynamic wheel load calculated for the experiment was around 1.3 times greater than the design for a high-speed train traveling at 350 km/h. An actuator mounted on the main sleeper's rail—which was placed between 5 sleepers—was used to methodically apply the dynamic pressure. Two stages comprised the dynamic loading test: an extended loading stage with 400,000 sinusoidal forces at 6 Hz, and a starting stabilizing stage with 3000 sinusoidal loads at 1 Hz [31–34]. This robust methodology ensures a comprehensive evaluation of the track's dynamic response under simulated operational conditions, providing valuable data for subsequent analyses and comparisons between the "control" and CAM-reinforced sections.

The average values, indicative of phase shifts, were employed for comprehensive plastic settlement analysis. Additionally, the strain amplitude (elastic strain) was computed as the difference between the maximum and minimum values, providing valuable insights for plastic strain analysis. This detailed analysis of dynamic load test measurements contributes to a nuanced understanding of the track's response to cyclic loading, facilitating a robust comparison between the "control" and CAM-reinforced sections.

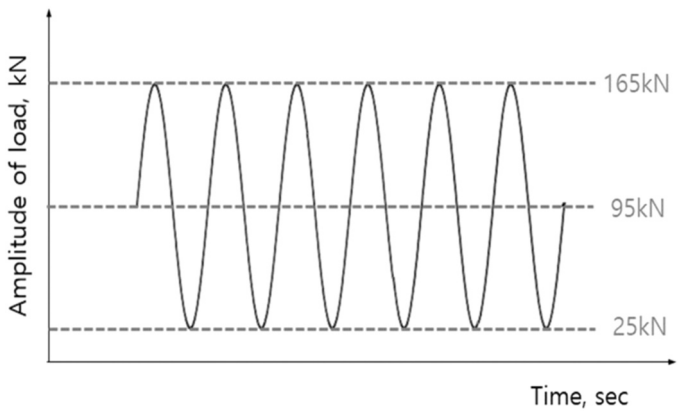

Fig. 5. Dynamic Load Test Method.

2.2. Laboratory test results

2.2.1. Light falling weight deflectometer (LFWD)

The small impact load test, executed with the LFWD, precisely mirrored the position delineated in Fig. 6 congruent with the copper plate load test position. Following three meticulously controlled loads, the resultant calculated elastic modulus values were meticulously averaged. The ensuing findings, as encapsulated in Table 3, unveiled a discerning average elastic modulus of 18.8 MPa. This LFWD assessment stands as a testament to the comprehensive methodologies employed in gauging the elastic properties of the track structure. The LFWD, with its precision and efficiency, offers a nuanced perspective on the material's capacity to withstand dynamic loads, contributing vital information to the overarching evaluation of track performance and material resilience.

2.2.2. Indoor compaction test

The soil roadbed, constituting the bedrock of the railway infrastructure, underwent meticulous scrutiny through an indoor compaction test, ensuring a profound understanding of its structural integrity. Commencing with a thorough drying process lasting 24 hours within a specialized drying furnace, the dried samples were subjected to the D compaction method. Employing an automatic compactor following the KS F 2312 standard, the compaction procedure adhered to stringent specifications, utilizing a carefully selected mold, color, base plate, and spacer disk. The sample preparation involved a meticulous drying method, and the compaction test followed a repeat method, offering consistency and reliability in the analytical process. For an 8 kg dry sample, incremental increases of approximately 2% in water content were meticulously executed, spanning a total of 5 iterations to construct a comprehensive compaction curve. This indoor compaction analysis stands as a pivotal component in delineating the soil roadbed's responsiveness to compaction efforts, providing essential insights for track design and structural optimization. The obtained results include the Optimum Moisture Content (OMC) at 9.25%, the maximum dry density (γ dmax) at 2.08 g/cm^3, and the 95% of γ dmax at 1.976 g/cm^3.

2.2.3. Field density test (FDT)

A meticulous evaluation of on-site compactness was undertaken through the FDT at the designated location, as depicted in Fig. 7. The finished surface of the soil roadbed served as the testing ground (see Fig. 7a), where a base plate, conforming to the KS F 2311 standard, was firmly secured with nails to prevent any inadvertent movement (see Fig. 7b). The test protocol involved the excavation of the base plate's interior using a chisel, facilitating the collection of a requisite sample for the field density test. To ascertain the volume of the excavated section, standard yarn was used for replacement with the aid of a density meter (see Fig. 7c). The excavation volume was quantified by measuring the weight of the substituted standard yarn. Following the collection, the sample underwent a 24-hour drying process in a drying furnace to determine its moisture content. Subsequently, the compaction degree was calculated utilizing the compaction result value. The on-site resolution level was gauged at 91.1%, showcasing a notable alignment with contemporary railroad design standards, signifying the adherence to prevailing industry benchmarks.

2.3. Numerical simulation

2.3.1. Overview

The intricate behaviors of deteriorated ballast reinforced by cement asphalt mortar take center stage in this segment, leveraging the robust capabilities of the commercial program ABAQUS. The essence of this simulation lies in the emulation of a running train traversing a simplified railway structure. Moreover, the efficacy of the cement asphalt mortar stabilization technique stands juxtaposed with the performance of the deteriorated ballast track. The selection of the optimal cement asphalt mortar, identified through prior laboratory experiments, underscores the precision of the numerical simulation. Illustrated in Fig. 8a, a specific section within the reinforcement zone is meticulously crafted to scrutinize the effectiveness of cement asphalt mortar deployment. Embracing a pragmatic approach, the study opts for a 3D model to streamline the analysis, as showcased in Fig. 8b, for the complete running train model.

Delving into cyclic load analysis, both 2D and 3D models are meticulously devised, addressing the adaptability of a small railway

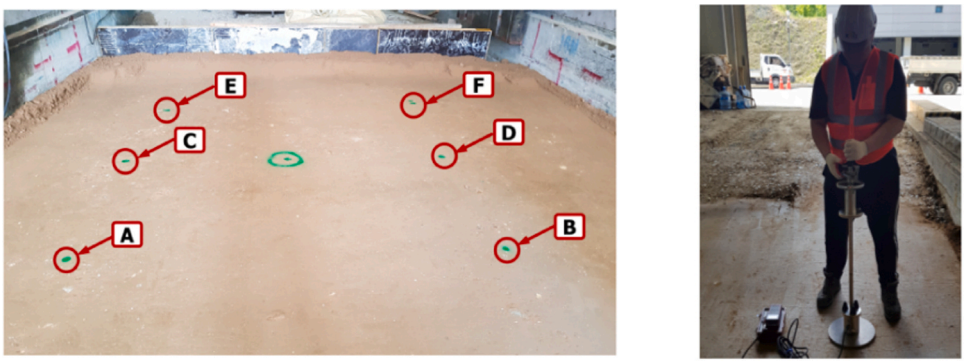

Fig. 6. LFWD test locations.

Table 3
LFWD test results.

Locations	Modulus of elasticity (E_{LFWD}, MN/m^2)	Position average (MN/m^2)	Overall average (MN/m^2)
A	21	22.67	18.89
	23		
	24		
B	18	19.33	
	20		
	20		
C	17	18.67	
	19		
	20		
D	17	18.33	
	19		
	19		
E	19	19.67	
	20		
	20		
F	14	14.67	
	15		
	15		

Fig. 7. Field density test.

structure for cyclic loading simulations. The dimensions of the railway structure and its components draw inspiration from recommendations by the Korean Railway Research Institute [35] and pertinent literature [36]. The model's length, strategically set at 482 m, aims to minimize boundary effects emanating from the embankment positioned behind the abutment. Within the purview of this research, two distinct railway tracks take the forefront: the deteriorated ballast track and the CAM-reinforced ballast track. The numerical modeling intricacies encompassing the train and bogies are encapsulated in Fig. 9, offering a comprehensive glimpse into the simulation framework, complemented by the detailed specifications delineated in Table 4 and Table 5.

2.3.2. *Boundary and mesh characteristics*

The horizontal constraints apply to the remaining elements of the model, but the foundational base is established as entirely fixed to prevent displacement in determining the numerical model's trustworthiness. The mesh size is carefully chosen after conducting several trials, with a denser arrangement in regions that are essential for closely examining important communities. The element count is limited to 21,300 because any number over this amount resulted in insignificant settlements. The 4-node bilinear plane strain quadrilateral (CPE4) was selected in accordance with accepted industry practices. Using knowledge from well-established literature, a frictionless configuration with tangential behavior and a strong hard contact mechanism in the normal direction are chosen for layer interfaces. In a number of interfaces, a surface tie contact is used to speed up simulation analysis. Together, these factors guarantee the resilience and correctness of the numerical model, paving the way for a thorough examination of its behavior.

2.3.3. *Materials Inputs*

In delineating the simulation framework, meticulous attention is given to material inputs, specifically tailoring parameters (i.e., ϕ, ψ) for the ballast layer. Embracing the Drucker-Prager/Cap yield criterion, a well-established choice in pertinent literature [37], ensures a nuanced representation of ballast behavior within the virtual environment. In the pursuit of convergence stability throughout the simulation, a judicious selection is made for the cohesion (C) value, strategically pegged at approximately 1kPa. Simultaneously, the friction angle is deliberately set to 45°, a configuration aimed at enhancing the reliability and accuracy of the simulation outcomes. This approach is complemented by the utilization of an elastoplastic material exhibiting a constitutive model, thoughtfully chosen to mirror the inherent characteristics of the flowable soil mixture incorporated in the study. Table 6 summarizes the properties of the materials used in the simulation method [5,36,38,39].

The mesh sensitivity analysis in Table 7 examines the influence of the number of elements on the settlement at the end of the approach slab, with a backfill solution using lightweight soil. The settlement values follow a consistent pattern, showing a gradual decrease with an increasing number of elements. Starting with 675 elements, the settlement is noted at −3.9 mm, and as the mesh density rises, the settlement becomes more negative, reaching −4.422 mm with 63,800 elements. This indicates a tendency toward

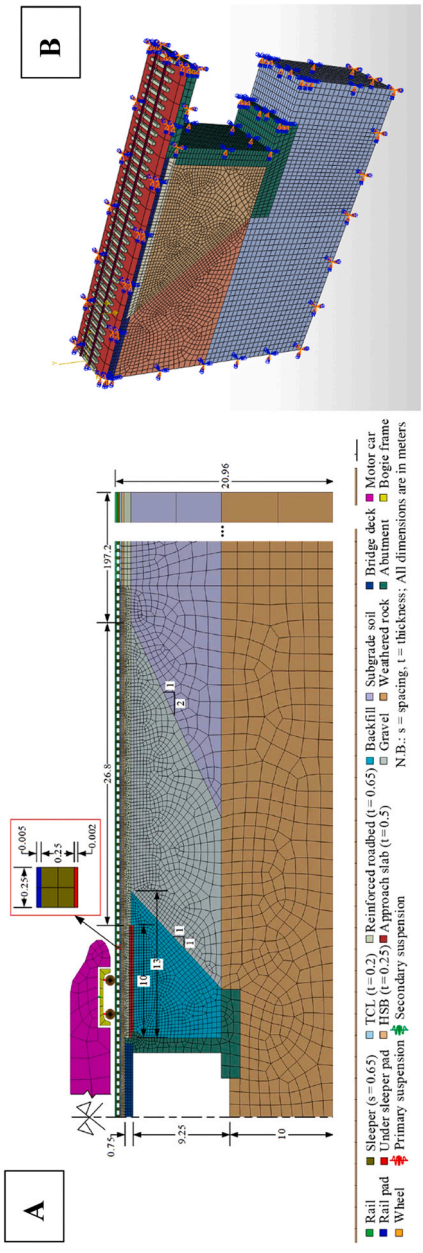

Fig. 8. 2D & 3D Modelling of simple railway structure.

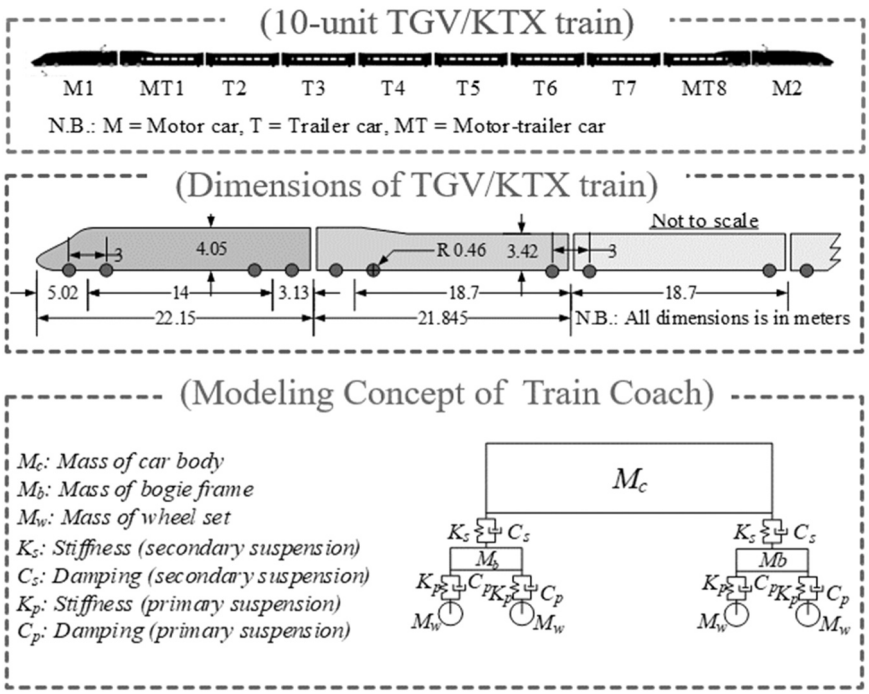

Fig. 9. Finite element modeling of TGV/KTX train.

Table 4
Basic mass properties of the train.

Part	Component	Mass (kg)
Motor car	Car body	53,580
	Bogie frame	2945
	Wheelset	2130
Trailer car	Car body	26,750
	Bogie frame	3140
	Wheelset	1725

Table 5
Basic stiffness/damping properties of suspensions.

Part	Component	Parameter	Value	Unit
Motor car	Primary suspension	Stiffness	1.418	MN/m
		Damping	9.2	kNs/m
	Secondary suspension	Stiffness	1.695	MN/m
		Damping	11.8	kNs/m
Trailer car	Primary suspension	Stiffness	0.525	MN/m
		Damping	8.1	kNs/m
	Secondary suspension	Stiffness	0.465	MN/m
		Damping	29.5	kNs/m

greater settlement with finer mesh resolution. However, it's noteworthy that beyond a certain point, the changes in settlement become marginal, suggesting the attainment of mesh convergence. Mesh sensitivity analysis is pivotal for striking a balance between computational efficiency and accuracy, ensuring that the chosen mesh provides dependable results without unnecessary computational overhead.

2.3.4. Loading condition

Drawing upon insights gleaned from antecedent research endeavors [5,20,38,40] and informed by recommendations from the Korean Railroad Research Institute [41], the loading condition in the simulation is meticulously constructed. The concentrated force exerted by the train wheel is adeptly designed to approximate the central force, aligning harmoniously at approximately 171.6 kN. This particular value is emblematic of the dynamic wheel load induced by the KRL-2012 Cargo/Passenger train variant, operating at a

Table 6
Materials Properties for Numerical Simulation.

Material	Unit weight (kN/m^3)	Elastic Modulus (MPa)	Poisson's ratio	Thickness (m)
Reinforced roadbed	20	120	0.21	0.4
Stabilized Ballast layer	16	300	0.3	0.4
Ballast layer	15	150	0.3	0.4
Subgrade layer	19	80	0.3	10
Sleeper	24	20,000	0.2	0.25
Weathered rock layer	20	100	0.2	10
Rail	49	210,000	0.3	0.15

Table 7
Mesh Sensitivity Analysis.

No. of Elements	Settlement at the End of Approach Slab (mm)
675	-3.9
5500	-4.1
11,200	-4.35
22,000	-4.4
48,500	-4.41
63,800	-4.422

velocity of 140 km/h. Such precision in loading condition specification underscores the fidelity of the simulation to real-world scenarios, enhancing the reliability and relevance of the obtained results.

3. Results and discussions

3.1. Full train running analysis

The settlement characteristics are scrutinized in Fig. 10, providing a comparative evaluation between the deteriorated ballast track with and without CAM stabilization. The Finite Element Method (FEM) results unveil a parallel trend in settlement distribution for both ballasted tracks. Particularly noteworthy is the observation that, under the influence of a single train load, critical settlement values are evident around 1 and 3 seconds into the train's movement, corresponding to the passage of the train head (motor car) through the monitored point. After these critical points, settlement values tend to be milder under the trailer cars. Further exploration of the numerical results underscores a pronounced disparity in settlement between the two scenarios. The CAM-reinforced ballast exhibits a remarkable improvement compared to the control section, particularly discernible under the influence of a single train run. This enhanced performance is attributed to the robust elastic modulus of the CAM-reinforced ballast layer, significantly bolstering the stress-bearing capacity of the entire railway structure.

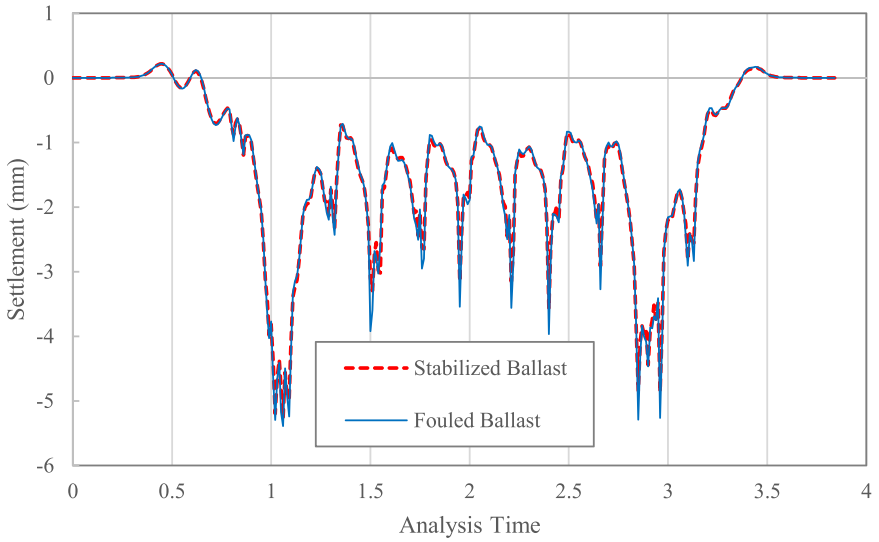

Fig. 10. The settlement response of the ballasted track under full train running.

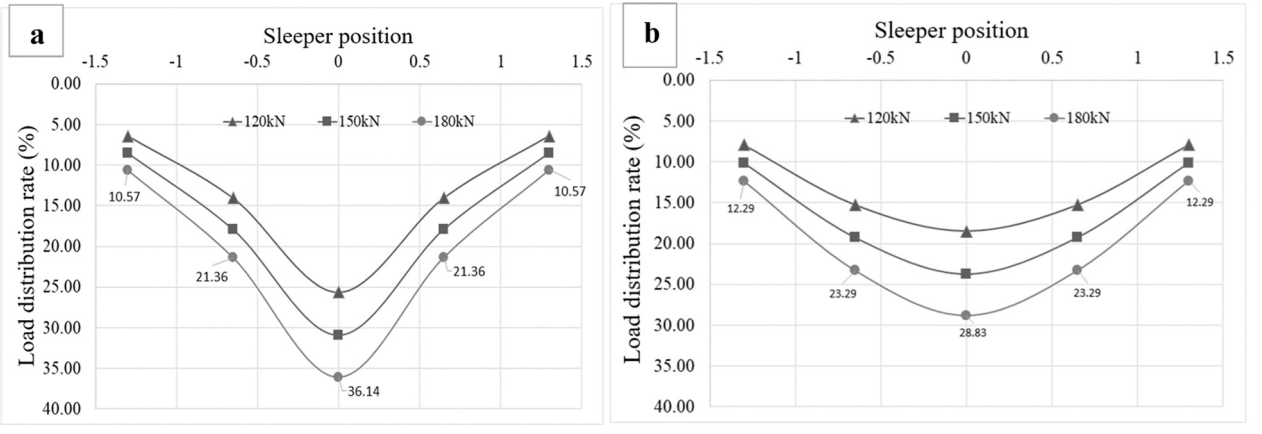

Fig. 11. Load distribution (Prior to the Dynamic Load): (a) control zone & (b) CAM-reinforced zone.

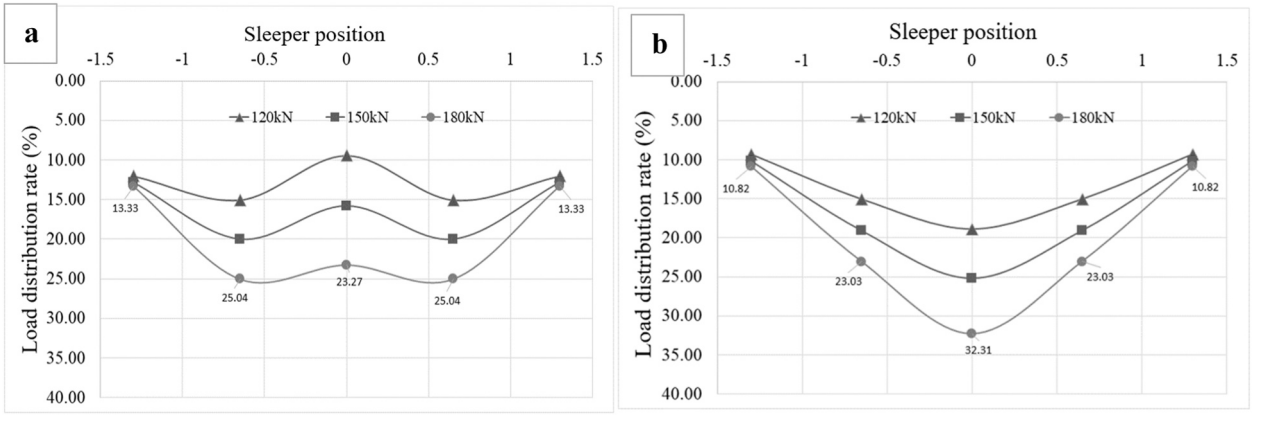

Fig. 12. Load distribution (After the Dynamic Load): (a) control zone & (b) CAM-reinforced zone.

3.2. Distribution of load ratio according to sleepers

The investigation into features of the load allocation during static loading, as illustrated in Fig. 11 and Fig. 12, sheds light on the effects of separation distance from the loading point at varying load levels (120 kN, 150 kN, and 180 kN). Before dynamic loading, the control track exhibits a relatively higher load distribution ratio directly beneath the sleeper compared to the reinforced track. This disparity is attributed to the superior loading transfer capability of the reinforced track with CAM, facilitating more efficient static load sharing across the sleeper system. The reference track shows a substantial reduction in the load allocation proportion during dynamic load testing, from 36.14% to 23.27% just below the loading mark. As previously mentioned, this decrease is a sign of the floating sleeper's effects. While the distribution proportion for nearby sleepers stays similar with pre-dynamic loading conditions, the load distribution ratio in the CAM-reinforced track tends to increase from 29.11% to 33.47% at the middle sleeper. This nuanced observation underscores the stabilizing influence of CAM, improving the durability of the deteriorated ballast trackbed.

3.3. Cyclic load analysis (2D)

Fig. 13 depicts the displacement characteristics of the deteriorated ballast track system under 400,000 cyclic loads, as analyzed through the 2D numerical simulation. The results showcase a consistent alignment with measurements obtained from the full-scale testing. Upon close examination of the modeling, it becomes evident that the plastic displacement of the deteriorated ballast track experiences a rapid increase within the initial 10,000 cycles, reaching a magnitude of nearly 3.5 mm. This substantial settlement signifies the initial compaction of the ballast volume. Subsequently, the plastic displacement demonstrates a gradual escalation at a more moderate rate, reaching approximately 4.5 mm after 200,000 cycles. The concluding phase can be interpreted as a stable settlement, as the overall displacement of the deteriorated ballast track undergoes a gradual increase of 0.5 mm in the last cycle.

The results of the 2D numerical modeling for CAM-reinforced ballast are presented in Fig. 13, showcasing a close correspondence with measurements derived from full-scale experiments. Upon closer examination, the initial settlement in the CAM-reinforced ballast

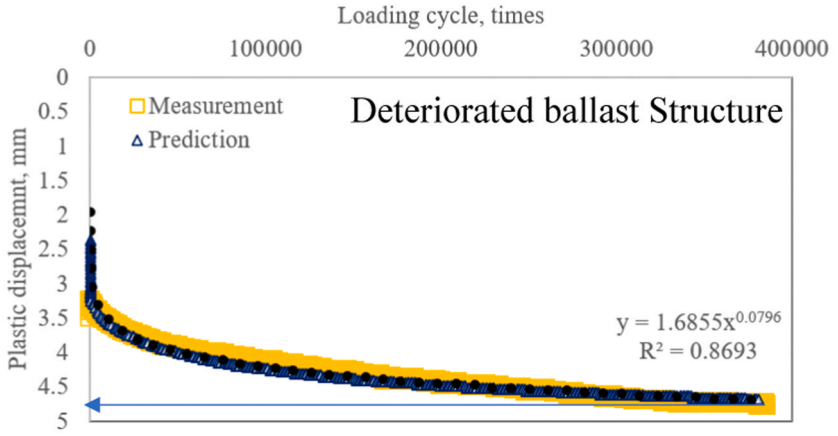

The plastic displacement comparison of deteriorated ballast structure (2D).

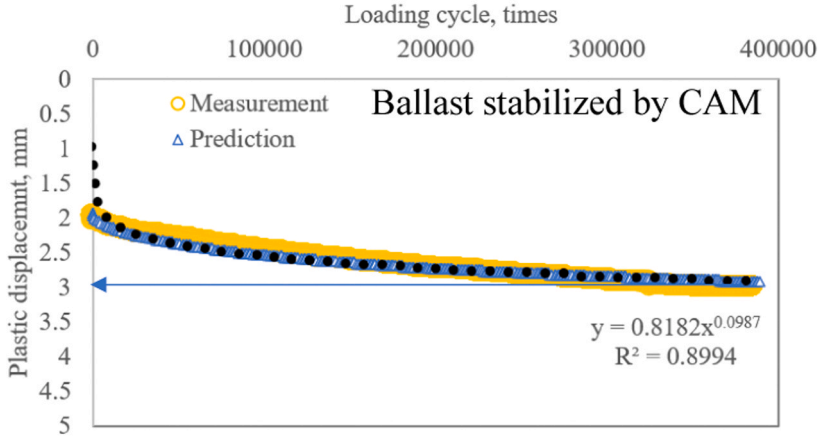

Fig. 13. The plastic displacement comparison of new ballast structure (2D).

is noticeably retarded, exhibiting a reduction of 33% when compared to the controlled track. This enhancement in settlement resistance aligns with the effectiveness of the CAM stabilization technique. Furthermore, during the 2nd and last stages of loading, the displacement of the deteriorated ballast track is shortened by 0.5 mm compared to the previous condition. This observation supports the conclusion that the CAM stabilization technique is indeed effective in reinforcing the deteriorated ballast track, demonstrating improved settlement resistance and enhanced durability under cyclic loads.

Assessing the efficacy of the 2D prediction, a thorough analysis of both anticipated and actual values in the context of degraded ballast reveals a distinctive pattern. There is a discernible surge in plastic displacement within the initial 50,000 loading cycles, attributed to the compacted nature of the ballast-filling air voids between particles, increasing from up to 4 mm. Following this initial phase, the plastic displacement experiences a gradual ascent, stabilizing at around 4.8 mm. In stark contrast, the new ballast structure exhibits a more restrained plastic settlement, measuring at less than 2.4 mm during the initial 50,000 cycles—an evident reduction of 50% compared to its degraded counterpart. The ultimate plastic settlement in the new ballast hovers around 3.0 mm, reflecting a notable 40% decrease compared to the degraded ballast. These consistent patterns between predicted and measured values robustly affirm the reinforcing efficacy endowed by the CAM stabilization method. This innovative technique not only curtails plastic displacement but also ensures a more resilient and stable railway track structure, as substantiated by the convergence of anticipated and observed outcomes.

The colormap depiction in the 2D simulation method offers a lucid understanding of the experimental findings as shown in Fig. 14. It validates that the CAM reinforcement ballast technique guarantees a consistent and well-distributed load across the entire structure as shown in Fig. 14a. In contrast, the conventional method exhibits a conspicuous concentration of displacement at the central sleeper, signaling a pivotal stress point (see Fig. 14b). This visual representation underscores the efficacy of the CAM reinforcement ballast method in establishing a uniform and stable stress distribution throughout the railway track structure in the 2D simulation.

3.4. Cyclic load analysis (3D model)

The 3D modeling predictions for the plastic displacement of deteriorated ballast structure are presented in Fig. 15, showcasing a robust correlation with the actual measurements obtained from experimental tests. The 3D prediction, in alignment with the observed measurements, illustrates a critical settlement occurring within the initial 10,000 cycles. Subsequently, the entire track system undergoes a stable reduction in settlement for the remaining cyclic load duration. A complicated interplay of elements controlling settlement behavior may be seen in the progressive settlement observed in the previous cycles, which may be explained by the strong bond between ballast particles and a decrease in the air-void system within the deteriorating ballast.

The 3D simulation of the CAM-reinforced ballast structure demonstrates a compelling fit with the measurements obtained from the full-scale testing, as illustrated in Fig. 15. Building upon insights from the 2D modeling analysis, the incorporation of CAM into the deteriorated ballast structure yields significant improvements in structural integrity. CAM effectively permeates the air-void spaces among deteriorated ballast particles, contributing to the partial restoration of the layer's strength. The stress dissipation capabilities of the asphalt binder, coupled with the stress-bearing capacity of the cement hydration process, collectively enhance the displacement resistance of the deteriorated ballast structure by up to 33%. The contour maps presented in Fig. 16 underscore the homogeneous distribution of loads facilitated by the CAM stabilization method along the railway structure, effectively dissipating stress from the central force to the adjacent regions. Notably, the main sleeper emerges as a pivotal stress-bearing component in the deteriorated ballast system. This observation substantiates the accelerated degradation of the deteriorated ballast track system and validates the rehabilitative potential of the CAM technique.

In the realm of degraded ballast, a comprehensive examination of both predicted and measured values unveils a noteworthy trend: a discernible surge in plastic displacement within the initial 50,000 loading cycles. This phenomenon, attributed to the compacted nature of the ballast filling air voids between particles, manifests as an increase of up to 4 mm. Subsequently, the plastic displacement experiences a gradual ascent, stabilizing at approximately 5 mm. In stark contrast, the new ballast structure exhibits a more restrained plastic settlement, registering at less than 2.5 mm during the initial 50,000 cycles—an evident 60% reduction compared to its degraded counterpart. The ultimate plastic settlement in the new ballast hovers around 2.8 mm, reflecting a notable 44.44% decrease compared to the degraded ballast. These consistent patterns between predicted and measured values provide robust evidence of the

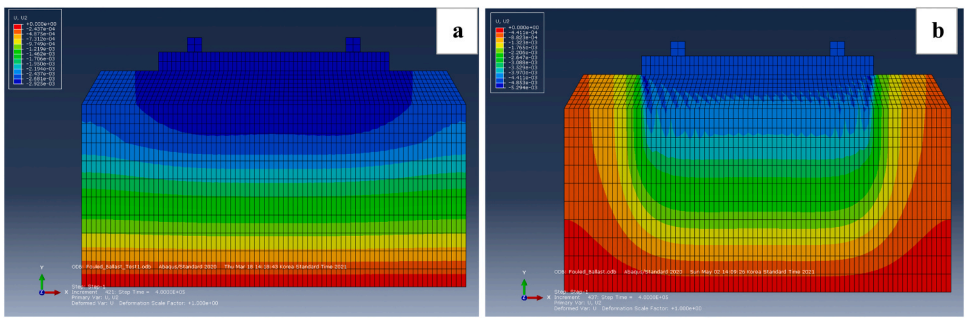

Fig. 14. The settlement comparison between CAM reinforced ballast (a) and deteriorated ballast (b) using 2D modeling.

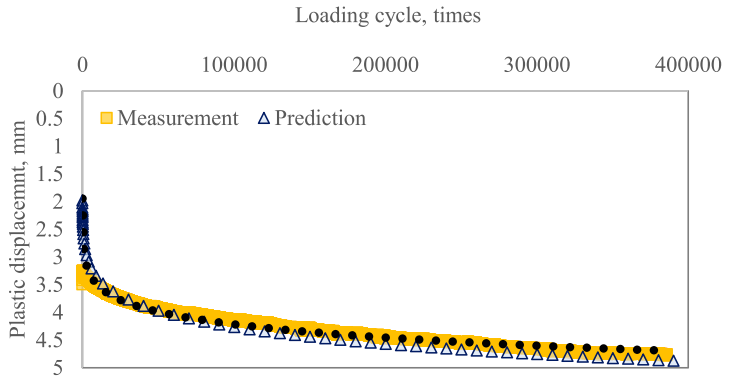

The plastic displacement comparison of deteriorated ballast structure (3D Model).

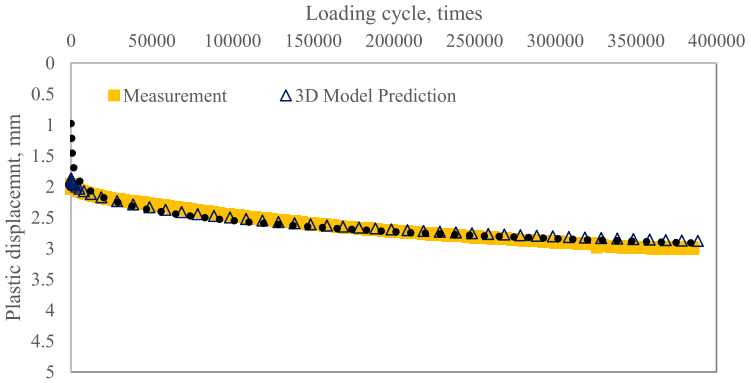

The plastic displacement comparison of deteriorated ballast stabilized by CAM (3D Model).

Fig. 15. The plastic displacement comparison of deteriorated ballast stabilized by CAM (3D Model).

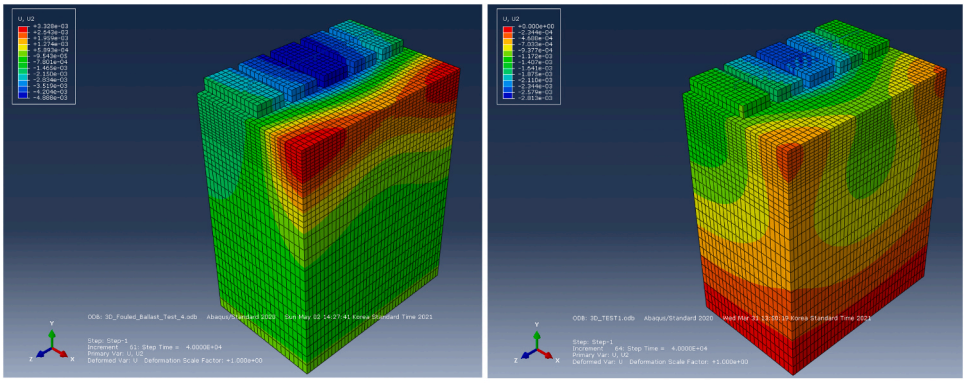

(a) Deteriorated ballast (b) Stabilized Ballast

Fig. 16. The settlement comparison between CAM reinforced ballast (a) and deteriorated ballast (b) using 3D modeling.

reinforcing prowess endowed by the CAM stabilization method. The innovative technique not only curtails plastic displacement but also ensures a more resilient and stable railway track structure, as substantiated by the convergence of anticipated and observed outcomes.

The colormap representation in the simulation method provides a clear insight into the test results. It confirms that the CAM reinforcement ballast method ensures a smooth and even distribution of load throughout the entire structure. On the other hand, the

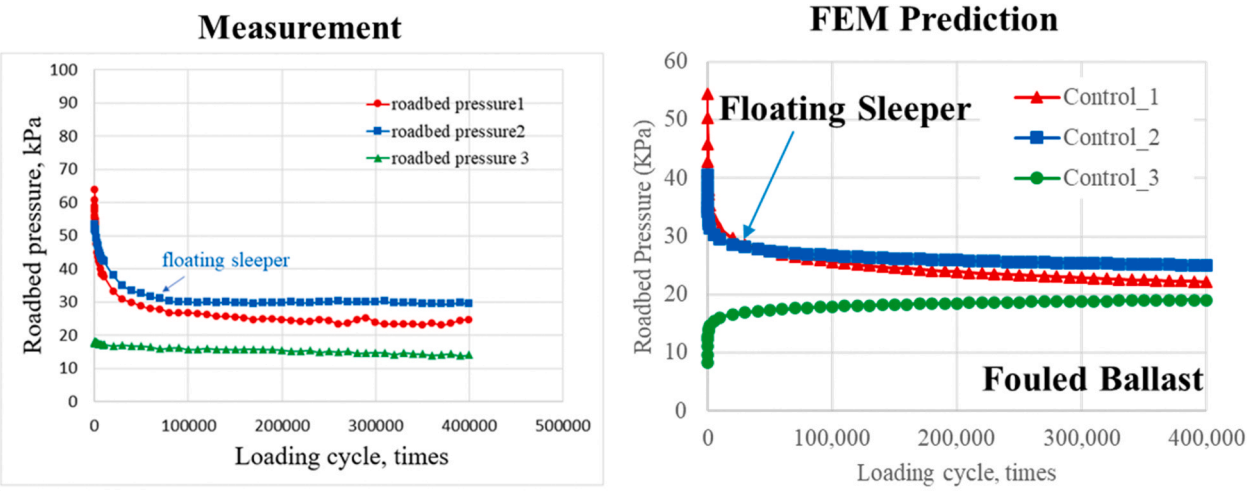

(a) Actual measurement vs (b) FEM prediction of control section.

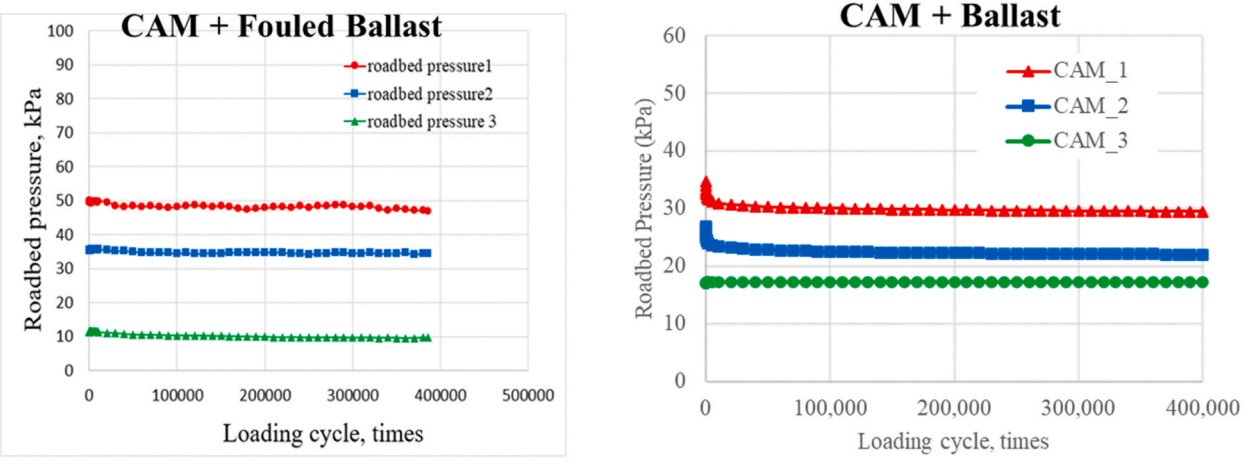

(c) Actual measurement vs (d) FEM prediction of CAM section.

Fig. 17. Roadbed pressure under cyclic load.

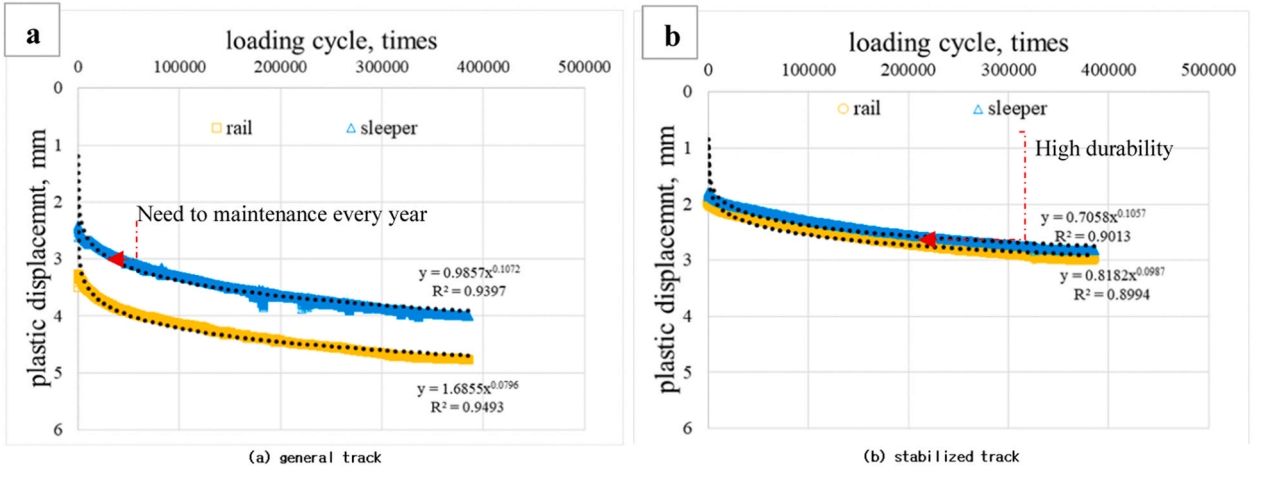

Fig. 18. Control zone (a) and reinforced zone(b) show plastic deformation under load repetition.

conventional method results in a noticeable concentration of displacement at the central sleeper, indicating a critical stress point. This visual representation makes it evident that the CAM reinforcement ballast method is effective in achieving a uniform and stable stress distribution across the railway track structure.

As presented in Fig. 17, the comparative analysis between the simulation and the outcomes derived from the full-scale test bed consistently underscores the prevalent floating issue beneath the concrete slab of the railway track. Examining the conventional method reveals a problematic stress concentration on the sleeper due to inadequate stress distribution within the underlying ballast. This irregular distribution is further evidenced by the significant discrepancy in roadbed pressure, with a pronounced decrease at the lower layer juxtaposed with a substantial increase at the upper layer.

In stark contrast, the reinforcement method portrays a more favorable scenario characterized by a notably smoother stress distribution. The elevated roadbed pressure in this context serves as a reliable indicator of the absence of a floating sleeper, implying the successful elimination of voids between the sleeper and the underlying ballast. This positive outcome is intricately tied to the stabilizing effects of the CAM mixture, fostering cohesion among discrete ballast particles. The resultant fully connected layer, extending seamlessly from the top to the bottom, plays a pivotal role in efficiently transferring wheel loads to the compacted soil layer beneath. This not only mitigates the floating issue but also significantly enhances the overall durability and structural integrity of the railway track.

The manifestation of the floating sleeper issue becomes evident upon closer examination of the dataset extraction, particularly in the roadbed pressure readings of adjacent sleepers relative to the main sleeper. Specifically, roadbed pressures 2 and 3, situated progressively farther from the main sleeper (roadbed pressure 1), exhibit significant variations. This observation is particularly pronounced during the 10,000–50,000 loading cycles. In the deteriorated ballast scenario, a notable reduction in roadbed pressure at positions 1 and 2 is discernible, indicative of the floating sleeper effect. Simultaneously, roadbed pressure at position 3 experiences a substantial increase, bearing the additional load from the main sleeper. For instance, the roadbed pressure in the control section diminishes from 65 kPa to approximately 28 kPa within the initial 50,000 cycles. This reduction is similarly observed in the simulation section, with roadbed pressure dropping from 55 kPa to around 28 kPa. Notably, an increase in roadbed pressure at position 3 is evident in the simulation zone.

Conversely, in the reinforced section, stable roadbed pressures of approximately 50 kPa, 36.5 kPa, and 10 kPa are recorded for positions 1, 2, and 3, respectively, in the full-scale testing zone. Predicted values closely align, measuring around 30 kPa, 23.5 kPa, and 18 kPa for the corresponding positions. The consistency in roadbed pressure stability is confirmed in both sections. However, a slight reduction in roadbed pressures 1 and 2 is noted in the simulated zone, suggesting the need for further refinement in future simulation studies. Overall, the dataset strongly supports the conclusion that the significant reduction in roadbed pressure, attributable to the floating sleeper phenomenon, is a validated and substantial concern.

3.5. Life cycle cost analysis results and discussion

The results obtained from the full-scale testing, as shown in Fig. 18, highlight a significant improvement in the track structure's longevity with the use of CAM. One example worth mentioning is the sleeper's plastic deformation on the control track, which reached 3 mm in just 4000 cycles. In contrast, this magnitude of deformation is attained in the CAM-reinforced track after a considerably prolonged period of 400,000 cycles. This stark contrast in performance highlights the pronounced longevity and resilience imparted by CAM stabilization, paving the way for an insightful discussion on the life cycle cost implications of this innovative track reinforcement method.

A methodical strategy for constructing, preservation, and replacement plans for both control and consolidated segments has been rigorously developed, based on the extensive examination of the full-scale experimentation findings. Table 8 presents the LCCA organizational structure that outlines the chronological sequence of operations related to construction, preservation, and replacement. The control segment requires minimal repair work once a year, as required by the strict deviation threshold of a maximum of 3 mm, according to the results of the LCCA method. Additionally, reconstruction procedures are deemed necessary every 20 years to ensure the sustained performance of the track structure. In contrast, the stabilized section exhibits a more extended maintenance cycle, requiring minor interventions every decade. The reconstruction imperative arises every 30 years, underscoring the enduring stability and prolonged service life attributed to the innovative CAM stabilization approach. This strategic delineation serves as a valuable guide for optimizing the life cycle costs associated with the track infrastructure, aligning maintenance efforts with the specific needs of each track section.

Table 8
60-Year LCCA of construction and maintenance strategies.

Years	0	5	10	15	20	25	30	35	40	45	50	55	60
Control	*	*	*	*	***	*	*	*	***	*	*	*	***
CAM	**		**		**		****		**		**		****
Note:													
*	Control section minor maintenance: Ballast Tamping method												
**	Stabilized section minor maintenance: CAM method												
***	Reconstruction of the control section												
****	Reconstruction of CAM section												

3.5.1. Inflation Compensation Rate = 3.5% (or discount rate compensation)

Transitioning to the second phase of analysis, the inclusion of a 3.5% inflation compensation rate introduces a more dynamic aspect to the evaluation. In contrast to the initial scenario where the total construction and maintenance performance costs maintained an unchanging ratio, equation (5.4) highlights the evolving relationship. The introduction of the inflation compensation rate ensures that the total costs do not remain constant, accounting for the fluctuating economic landscape. This nuanced approach acknowledges the impact of inflation on construction and maintenance performance costs, providing a more realistic representation of the evolving economic conditions. As a consequence, the refined analysis with the inflation compensation rate aims to capture the inherent dynamics of economic variables and offer a more accurate portrayal of life cycle cost considerations.

$$\frac{(\text{construction} + \text{maintenance})\text{performance}}{(\text{construction} + \text{maintenance})\text{cost}}\text{atinitialyearishigherthan}$$
$$\frac{(\text{construction} + \text{maintenance})\text{performance}}{(\text{construction} + \text{maintenance})\text{cost}}\text{atthefollowingyear.} \quad (2)$$

In delineating the economic intricacies, the second analysis recognizes the necessity to address the influence of inflation on future costs. Consider a scenario where the initial rehabilitation cost stands at 100,000,000 KRW in the first year. However, the ensuing impact of inflation necessitates an adjustment in the subsequent year's rehabilitation cost to ensure an equivalent performance level. Expressed in equation (5.5), the "compensate rate" becomes a pivotal factor in determining the future value of rehabilitation costs. This formulation encapsulates the essence of maintaining consistent performance quality amidst the ever-changing economic landscape. By factoring in the compensation rate, the analysis endeavors to provide a more comprehensive understanding of how inflation influences future costs and, consequently, the life cycle cost implications for the ballast quality maintenance process.

$$\text{Future value} = \sum_{k=0}^{N} (\text{Agency} + \text{Operation cost})_k * (1 + x)^k \quad (3)$$

Agency costs in this research include projected costs for building, maintaining, or reconstructing in the future. The expenses incurred as a result of pavement service delays brought on by repair and reconstruction activities are primarily referred to as operation costs. In this framework, the variable x stands for the compensation rate, N for the number of years, and k for the expected year.

In a 60-year analysis, Fig. 19 highlights the contrast between conventional tamping and CAM-stabilized ballast. CAM reduces maintenance frequency by up to 10 times, resulting in a significant 79.7% cost reduction compared to conventional tamping. The analysis, rooted in empirical evidence and performance enhancement, advocates for the adoption of CAM-reinforced ballast as a transformative approach to bolster the sustainability and economic resilience of the railway system.

4. Conclusions

This study focuses on addressing the floating sleeper phenomenon in ballasted railway tracks by introducing Nonionic Cement Asphalt Mortar (CAM). Through comprehensive full-scale testing experiments, track performance is evaluated with and without CAM stabilization, showcasing its ability to create a robust membrane between ballast particles, reinforcing the track-bed structure. The study encompasses wheel load modeling, including static and dynamic simulations, train movement modeling, roadbed pressure analysis, load distribution, and track rigidity analysis. LCCA affirms CAM's cost-effectiveness, significantly reducing settlement and ensuring long-term durability. Utilizing ABAQUS for numerical simulations, the study demonstrates CAM's effectiveness in stabilizing deteriorated ballast. Moreover, the simulations reveal the capability to identify the floating sleeper phenomenon in the full-scale test bed, providing valuable insights for real-world applications.

- 2D numerical modeling reveals a 33% reduction in initial settlement in CAM-reinforced ballast compared to the control track, emphasizing CAM's efficacy in enhancing settlement resistance. The technique also reduces displacement by 0.5 mm in the deteriorated ballast track, showcasing improved settlement resistance and durability. Consistent patterns between predicted and measured values affirm CAM's effectiveness in ensuring a resilient and stable railway track structure.
- The 2D prediction analysis discerns a surge in plastic displacement within the initial 50,000 loading cycles for degraded ballast, reaching a 4 mm increase due to compacted ballast. Subsequently, plastic displacement gradually stabilizes at around 4.8 mm. In contrast, the new ballast structure exhibits restrained plastic settlement, measuring under 2.4 mm in the initial 50,000 cycles, marking a 50% reduction compared to degraded ballast. The ultimate plastic settlement in new ballast is around 3.0 mm, reflecting a notable 40% decrease compared to the degraded ballast. Consistent patterns between predicted and measured values strongly affirm CAM stabilization's efficacy, showcasing reduced plastic displacement and ensuring a more resilient and stable railway track structure.
- The dataset analysis reveals a prominent floating sleeper issue in roadbed pressure readings. Notably, roadbed pressures 2 and 3, farther from the main sleeper (pressure 1), exhibit significant variations during 10,000–50,000 loading cycles. In deteriorated ballast, pressures at positions 1 and 2 decrease, indicating the floating sleeper effect, while pressure at position 3 increases. For instance, in the control section, pressure drops from 65 kPa to 28 kPa in the initial 50,000 cycles. In the simulation section, a similar reduction is observed. Conversely, in the reinforced section, stable pressures of about 50 kPa, 36.5 kPa, and 10 kPa are recorded for positions 1, 2, and 3, respectively. Predicted values closely align. Although pressure reduction is noted in simulated zones, the dataset strongly supports the concern that the floating sleeper phenomenon causes substantial pressure to decrease.

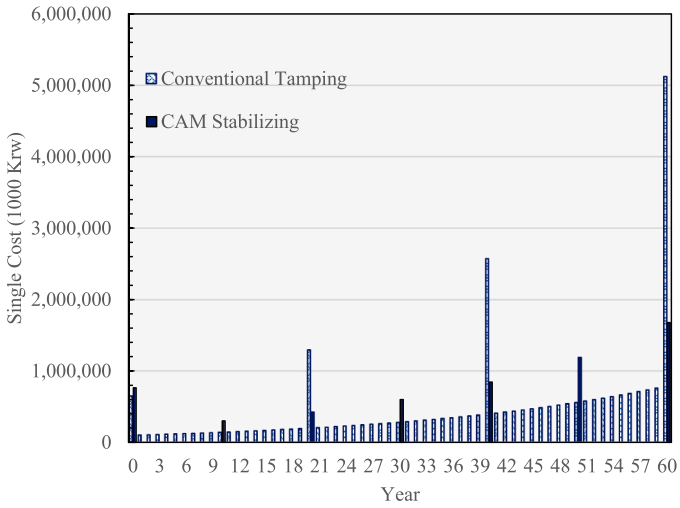

(a) Life Cycle Cost Analysis (60 years). (3.5% Compensate)

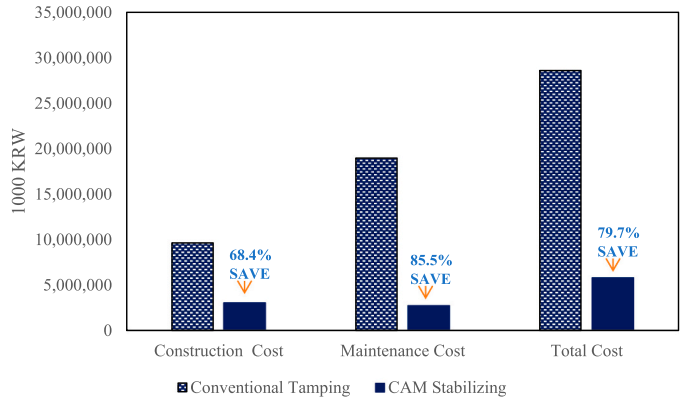

(b) Summary of Life Cycle Cost Comparison (60 years). (3.5% Compensate).

Fig. 19. (a) Life Cycle Cost Analysis (60 years). (3.5% Compensate). (b) Summary of Life Cycle Cost Comparison (60 years). (3.5% Compensate).

- The life cycle cost analysis (LCCA) provided a holistic perspective on the economic implications of the research. By comparing the conventional tamping method with the CAM-reinforced ballast approach, it was evident that the latter not only significantly reduced maintenance frequency but also exhibited a remarkable 79.7% reduction in the total cost over 60 years. This economic advantage, coupled with enhanced durability and performance, advocates strongly for the adoption of CAM stabilization as a transformative strategy in railway track maintenance.
- The study highlights a significant reduction in plastic displacement and enhanced stability attributed to the innovative CAM stabilization technique, underscoring its efficacy in minimizing the floating sleeper effect and ensuring the long-term durability of the railway track structure.
- The amalgamation of laboratory tests, numerical simulations, and life cycle cost analysis has offered a comprehensive understanding of the soil roadbed's behavior and the potential benefits of the cement asphalt mortar stabilization technique. These findings contribute to the ongoing discourse on optimizing railway infrastructure design, maintenance practices, and economic considerations. The research lays a robust foundation for further exploration and implementation of innovative approaches to enhance the sustainability and longevity of railway systems.
- In conclusion, the exploration of Nonionic CAM for ballasted railway track stabilization carries profound implications for both theoretical understanding and practical application. The study enriches theoretical frameworks by unveiling CAM's role in creating a robust membrane between ballast particles, contributing to the broader comprehension of soil-roadbed behavior. From a practical standpoint, key lessons emphasize CAM's efficacy in reducing settlement, enhancing durability, and mitigating the floating sleeper effect, offering a transformative approach to track maintenance. However, it is crucial to recognize the study's limitations, focusing primarily on CAM's stabilization efficacy and suggesting the need for future investigations into additional

influencing factors. This research sets the stage for advancements in railway engineering, bridging theory and practice for sustainable and resilient track infrastructure.

CRediT authorship contribution statement

Dae Wook Park, and Tri Ho Minh Le: Conceptualization, Methodology, Writing – original draft. **Dae Wook Park, Chanyong Choi, Tam Minh Phan, and Tri Ho Minh Le:** Visualization, Investigation, Writing – review & editing. **Chanyong Choi, Tam Minh Phan, and Tri Ho Minh Le:** Data curation, Software.

Declaration of Competing Interest

The authors whose names are listed immediately below certify that they have NO affiliations with or involvement in any organization or entity with any financial interest or non-financial interest in the subject matter or materials discussed in this manuscript.

Data Availability

Data will be made available on request.

Acknowledgments

This research was supported by a grant from the R&D Program (PK230B2) of the Korea Railroad Research Institute.

References

[1] A. Paixão, E. Fortunato, R. Calçada, Design and construction of backfills for railway track transition zones, Proc. Inst. Mech. Eng. Part F. J. Rail Rapid Transit. 229 (2015) 58–70, https://doi.org/10.1177/0954409713499016.
[2] E. Berggren, Railway Track Stiffness – Dynamic Measurements and Evaluation for Efficient Maintenance, Engineering (2009) 44.
[3] P. Hölscher, P. Meijers, Analysis of track and soil behavior at transition zones, (2009).
[4] I. Gallego, S. Sánchez-Cambronero, A. Rivas, E. Laguna, A mixed slab-ballasted track as a means to improve the behavior of railway infrastructure, Proc. Inst. Mech. Eng. Part F. J. Rail Rapid Transit. 230 (2016) 1659–1672, https://doi.org/10.1177/0954409715605128.
[5] T.H.M. Le, S.H. Lee, D.W. Park, Evaluation on full-scale testbed performance of cement asphalt mortar for ballasted track stabilization, Constr. Build. Mater. 254 (2020), https://doi.org/10.1016/j.conbuildmat.2020.119249.
[6] H. Wang, M. Silvast, V. Markine, B. Wiljanen, Analysis of the dynamic wheel loads in railway transition zones considering the moisture condition of the ballast and subballast, Appl. Sci. 7 (2017), https://doi.org/10.3390/app7121208.
[7] S. Costa D'Aguiar, E. Arlaud, R. Potvin, E. Laurans, C. Funfschillling, Railway transitional zones: a case history from ballasted to ballastless track, Int. J. Railw. Technol. 3 (2014) 37–61, https://doi.org/10.4203/ijrt.3.1.2.
[8] J. Ouyang, J. Zhao, Y. Tan, Modeling mechanical properties of cement asphalt emulsion mortar with different asphalt to cement ratios and temperatures, J. Mater. Civ. Eng. 30 (2018), https://doi.org/10.1061/(asce)mt.1943-5533.0002480.
[9] S. Jiang, J. Li, Z. Zhang, H. Wu, G. Liu, Factors influencing the performance of cement emulsified asphalt mortar – a review, Constr. Build. Mater. 279 (2021), https://doi.org/10.1016/j.conbuildmat.2021.122479.
[10] Y. Tan, J. Ouyang, J. Lv, Y. Li, Effect of emulsifier on cement hydration in cement asphalt mortar, Constr. Build. Mater. 47 (2013) 159–164, https://doi.org/10.1016/j.conbuildmat.2013.04.044.
[11] C. Alves Ribeiro, A. Paixão, E. Fortunato, R. Calçada, Under sleeper pads in transition zones at railway underpasses: numerical modeling and experimental validation, Struct. Infrastruct. Eng. 11 (2015) 1432–1449, https://doi.org/10.1080/15732479.2014.970203.
[12] K. Giannakos, S. Tsoukantas, Transition Zone between Ballastless and Ballasted Track: Influence of Changing Stiffness on Acting Forces, Procedia - Soc. Behav. Sci. 48 (2012) 3548–3557, https://doi.org/10.1016/j.sbspro.2012.06.1318.
[13] C. Ma, X. Zhao, J. Shi, J. Tao, H. Zhou, B. Dong, Y. Du, A rapid-hardening cement emulsified asphalt (CEA) mortar prepared from magnesium phosphate cement, J. Build. Eng. 76 (2023), https://doi.org/10.1016/j.jobe.2023.107312.
[14] A.H. Saesaei, A. Sahaf, S. Najjar, M.R.M. Aliha, Laboratory investigation on the fracture toughness (Mode I) and durability properties of eco-friendly cement emulsified asphalt mortar (CRTS II) exposed to acid attack, Case Stud. Constr. Mater. 20 (2024), https://doi.org/10.1016/j.cscm.2023.e02719.
[15] J. Ouyang, L. Hu, H. Li, B. Han, Effect of cement on the demulsifying behavior of over-stabilized asphalt emulsion during mixing, Constr. Build. Mater. 177 (2018) 252–260, https://doi.org/10.1016/j.conbuildmat.2018.05.141.
[16] Y. Tan, J. Ouyang, Y. Li, Factors influencing rheological properties of fresh cement asphalt emulsion paste, Constr. Build. Mater. 68 (2014) 611–617, https://doi.org/10.1016/j.conbuildmat.2014.07.020.
[17] J.C.O. Nielsen, X. Li, Railway track geometry degradation due to differential settlement of ballast/subgrade – Numerical prediction by an iterative procedure, J. Sound Vib. 412 (2018) 441–456, https://doi.org/10.1016/j.jsv.2017.10.005.
[18] D. Li, D. Davis, Transition of Railroad Bridge Approaches, J. Geotech. Geoenviron. Eng. 131 (2005) 1392–1398, https://doi.org/10.1061/(asce)1090-0241(2005)131:11(1392).
[19] S. Najjar, A. Mohammadzadeh Moghaddam, A. Sahaf, M.R.M. Aliha, Mixed mode-I/II fatigue performance of Cement Emulsified Asphalt Mortar: Experimental and statistical analysis at intermediate temperature, Constr. Build. Mater. 350 (2022), https://doi.org/10.1016/j.conbuildmat.2022.128835.
[20] T.H.M. Le, T.W. Lee, J.W. Seo, D.W. Park, Feasibility study of locally excavated soil in foamed cement mixture as backfill material for abutments of railway bridges, J. Test. Eval. 51 (2021), https://doi.org/10.1520/JTE20210169.
[21] J. Ouyang, H. Li, B. Han, The rheological properties and mechanisms of cement asphalt emulsion paste with different charge types of emulsion, Constr. Build. Mater. 147 (2017) 566–575, https://doi.org/10.1016/j.conbuildmat.2017.04.201.
[22] J. Ouyang, J. Zhao, Y. Tan, Modeling mechanical properties of cement asphalt emulsion mortar with different asphalt to cement ratios and temperatures, J. Mater. Civ. Eng. 30 (2018) 04018263, https://doi.org/10.1061/(asce)mt.1943-5533.0002480.
[23] C. Li, J. Ouyang, P. Cao, J. Shi, W. Yang, Y. Sha, Effect of rejuvenating agent on the pavement properties of cold recycled mixture with bitmen emulsion, Coatings 11 (2021), https://doi.org/10.3390/coatings11050520.
[24] ASTM D244, Standard test methods and practices for emulsified asphalts, Annu. B. Am. Soc. Test. Mater. Stand. 09 (2009) 1–8.
[25] ASTM C191, Standard test methods for Time of Setting of Hydraulic Cement by Vicat Needle, ASTM Int. (2019).
[26] ASTM C1097, Standard Specification for Hydrated Lime for Use in Asphalt Cement or Bituminous Paving Mixtures, ASTM Int. (2019).
[27] KSF 2374, Test method for dynamic stability of asphalt mixture, Korea Stand. Assoc. (n.d.).

[28] T.H.M. Le, D.W. Park, J.W. Seo, Evaluation on the mechanical properties of cement asphalt mortar with quick hardening admixture for railway maintenance, Constr. Build. Mater. 206 (2019) 375–384, https://doi.org/10.1016/j.conbuildmat.2019.02.104.
[29] Y. Meng, J. Ouyang, J. Ou, Investigation on the wetting behavior of asphalt emulsion on aggregate for asphalt emulsion mixture, Constr. Build. Mater. 400 (2023), https://doi.org/10.1016/j.conbuildmat.2023.132844.
[30] KRL-2012, Korea Rail Network Authority (2013). Design Standards for Railway Structures and Commentary, (2013).
[31] KR C-14030, Korea Railway Design Guidelines and Handbook – Ballasted Track Structure, Korea Rail Netw. Auth. (2018).
[32] KR C-14030, Railway design guide lines and handbooks (Ballasted Track Structure), Korea Railr. Netw. Auth. (2014).
[33] KR C-14030, Korea Railway Design Guidelines and Handbook, (n.d.).
[34] KR C-14040, Railway design guide lines and handbooks (Concrete Track Structure), Korea Railr. Netw. Auth. (2014).
[35] Korea Railroad Research Institute, Development of asphalt roadbed and track system suited to speed up, KRRI Rep. 2014 (2014).
[36] J.-Y. Kim, J.-H. Kim, K.-H. Cho, Assessment of stability of railway abutment using geosynthetics, Int. J. Railw. 9 (2016) 15–20, https://doi.org/10.7782/ijr.2016.9.1.015.
[37] M.M. Biabani, B. Indraratna, N.T. Ngo, Modelling of geocell-reinforced subballast subjected to cyclic loading, Geotext. Geomembr. 44 (2016) 489–503, https://doi.org/10.1016/j.geotexmem.2016.02.001.
[38] S.H. Lee, D.W. Park, H.V. Vo, M. Fang, Analysis of asphalt concrete track based on service line test results, Constr. Build. Mater. 203 (2019) 558–566, https://doi.org/10.1016/j.conbuildmat.2019.01.131.
[39] Ognibene G., Analysis of a bridge approach: long-term behavior from short-term response, (2019).
[40] S.H. Lee, H.V. Vo, D.W. Park, Investigation of asphalt track behavior under cyclic loading: Full-scale testing and numerical simulation, J. Test. Eval. 46 (2018), https://doi.org/10.1520/JTE20160554.
[41] KRRI, https://www.krri.re.kr/html/en/, (2019).